Taylor & Francis
Taylor & Francis Group

FAST SWITCHING OPTICAL MODULATOR BASED ON DUAL FREQUENCY NEMATIC CELL

Ye Yin, Mingxia Gu, Andrii B. Golovin, Sergij V. Shiyanovskii,
*and Oleg D. Lavrentovich**
Liquid Crystal Institute, Kent State University, Kent,
Ohio, 44242-0001, USA

We demonstrate a fast optical modulator capable of switching large amount of optical retardation (a few microns) in less than 1 ms. The result is achieved by employing a dual frequency nematic in cells with high pre-tilt alignment and by providing a special addressing scheme that features amplitude and frequency modulated voltage. We explore the effect of surface alignment and dielectric heating on the switching time. We also report the measurements of dielectric permittivities and crossover frequency of dual frequency nematic.

1. INTRODUCTION

Electrically-controlled liquid crystal (LC) cells are used in many modern optical applications that require switching of large optical retardation with short response time [1,2]. The two crucial parameters, the maximum optical retardation ΔL_{max} and the switching speeds ($\sim 1/\tau_{on}$, $\sim 1/\tau_{off}$) of the nematic LC cells depend differently on the cell thickness d setting the stage for necessary trade-offs [3]:

$$\Delta L_{\max} = (n_e - n_o)d, \tag{1}$$

$$\tau_{on} = \gamma_1 d^2/[\varepsilon_0|\Delta\varepsilon|(U_{rms} - U_c)], \quad \tau_{off} = \gamma_1 d^2/(\pi^2 K). \tag{2}$$

Here n_o, n_e are the ordinary and extraordinary refractive indices, respectively, K is the effective elastic constant, γ_1 is the characteristic rotational viscosity, $\Delta\varepsilon = \varepsilon_{||} - \varepsilon_{\perp}$ is the dielectric anisotropy, $\varepsilon_{||}$ and $\varepsilon_{\perp}$ are the dielectric permittivity components measured along and perpendicular to the

*Corresponding author. Tel.: (330) 672-4844, Fax: (330) 672-2796, E-mail: odl@lci.kent.edu

director, respectively; ε_0 is the permittivity of free space, U_c is the threshold voltage of Frederiks transition in a cell with planar or homeotropic alignment, and $U_{rms} > U_c$ is the actual applied voltage. The relevant figure of merit that depends on the switch-off time and characterizes the trade-off for the optical modulators,

$$FoM = \Delta L_{max}^2 / \pi^2 \tau_{off}, \tag{3}$$

can be re-expressed exclusively in terms of the material parameters [4]:

$$FoM_m = K(n_e - n_o)^2 / \gamma_1. \tag{4}$$

The latest expression inspired many researchers to seek for the improvement of optical retarders by synthesizing new materials with a higher optical birefringence, lower viscosity and larger Frank constants. Recently, our group has demonstrated that *FoM* can be improved by two orders of magnitude by exploring a different method of switching rather than synthesizing new materials [5]. The idea is to use dual frequency nematic (DFN) MLC2048 (EM Industries) in cells with high pre-tilt angle alignment and a special addressing scheme that features amplitude and frequency modulated voltage [5].

In this paper, we describe the technique briefly outlined in Reference [5], in a greater detail. In particular, we explore the effect of surface alignment and dielectric heating on the switching time of DFN cells. We also characterize the material properties of DFN such as dielectric permittivities, crossover frequency and rotational viscosity at different temperatures. We analyze the issue of dielectric heating, which is of special interest to DFN-based devices as the best mode of their operation might be achieved at elevated temperatures.

2. MATERIAL PROPERTIES OF DFN

Field-induced director reorientation depends on dielectric anisotropy $\Delta\varepsilon(f, T)$, which in DFNs changes its sign at a crossover frequency f_c. The quantities $\varepsilon_{||}$, $\varepsilon_\perp$, and f_c depend on the cell temperature T. We measured these dependencies for MLC2048 in planar and homeotropic cells with thickness about $15\,\mu\text{m}$. The pre-tilt angle in these and all other cells was measured by the magnetic null technique [6]. The cell was mounted in a hot stage permitting temperature stabilization within $0.1°\text{C}$. The complex impedance amplitude of the cell was measured by the Impedance/Gain-Phase Analyzer (model Schlumberger 1260) in the frequency range from $1\,\text{Hz}$ to $10\,\text{MHz}$ at voltage $0.5\,\text{V}$, in order to determine the dielectric permittivities of DFN.

Figure 1 shows $\varepsilon_{\parallel}$ and $\varepsilon_{\perp}$ as the functions of the applied voltage frequency at 20°C. The value of $\varepsilon_{\perp}$ does not change much in the frequency range (0.1–100) kHz while $\varepsilon_{\parallel}$ shows a dispersion region at relatively low frequencies (1–100) kHz. The intersection of two curves represents the crossover frequency, $f_c = 12\,\text{kHz} \pm 2\,\text{kHz}$ at T = 20°C. We independently determined f_c to be 12.9 kHz $\pm$ 0.2 kHz at 20°C by Senarmont method [7,8] (at f_c the cell becomes insensitive to the field and shows no optical response). The temperature dependence of $\varepsilon_{\perp}$ is shown in Figure 2.

We notice that f_c increases with temperature, for example, from 12 to 31 kHz when T changes from 20 to 32°C. At high temperature, $\Delta\varepsilon$ is always positive in broad frequency range of applied voltage as shown in Figure 3. The temperature behavior of f_c can be fitted by a straight line in the inverse-logarithmic coordinates, Figure 4, which implies that it is controlled by an activation process:

$$f_c \sim \exp(-E_f/k_B T), \tag{5}$$
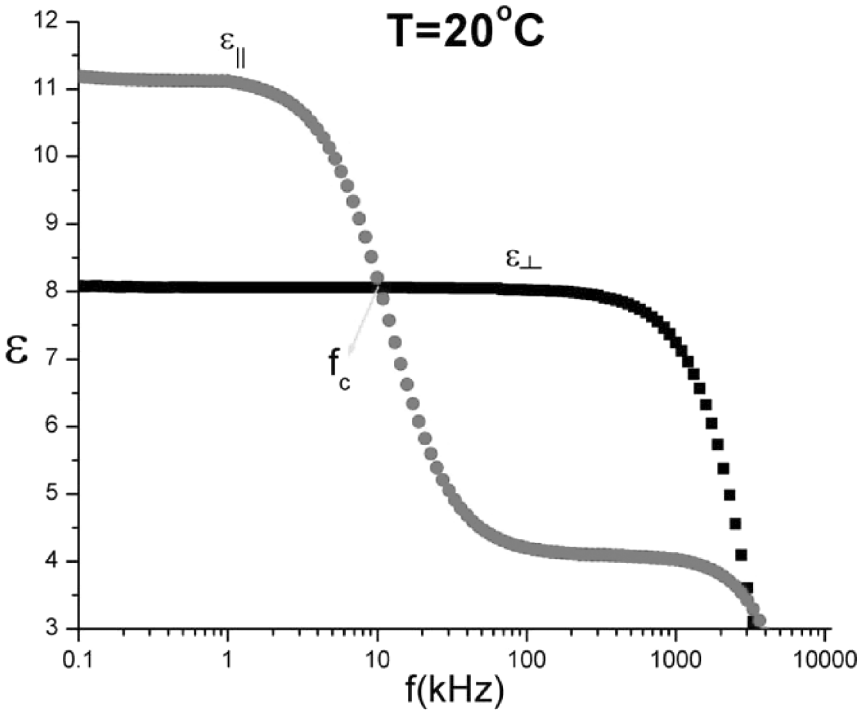
FIGURE 1 Frequency (logarithmic scale) dependent dielectric permittivities $\varepsilon_{\parallel}$ and $\varepsilon_{\perp}$ at 20°C.
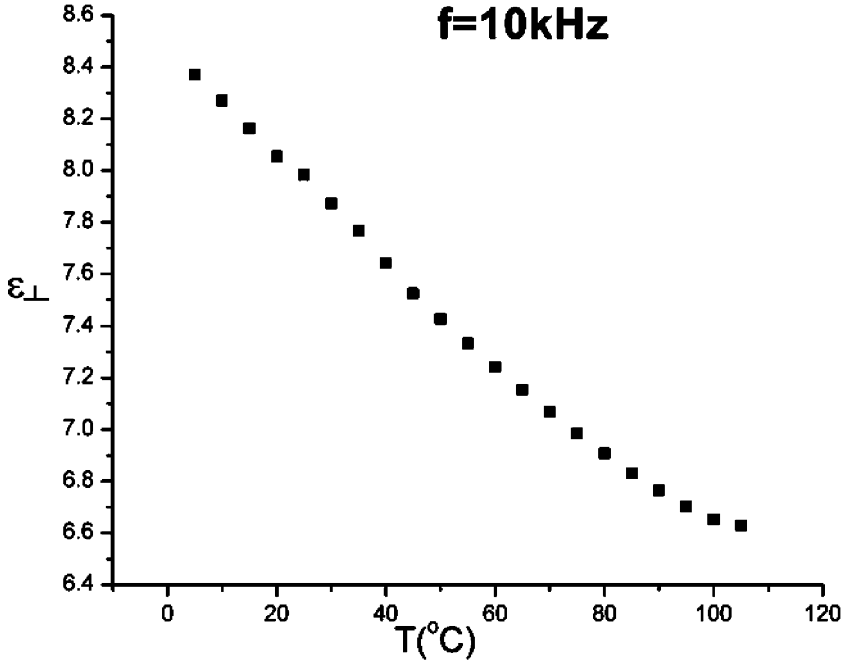
FIGURE 2 Dielectric permittivity $\varepsilon_\perp$ vs. temperature ($10°$C to $105°$C) at f $= 10$ kHz.

where k_B is the Boltzman constant and E_f is the activation energy representing the energy barrier associated with flip-overs of the long molecular axis. The linear fit in Figure 4 yields $E_f = 0.61$ eV.

The rotational viscosity γ_1 measured by the technique described in Reference [9] demonstrates the temperature dependence of the similar activation type [10], Figure 5:

$$\gamma_1 \sim S \cdot \exp(E_\gamma/k_B T) \tag{6}$$

Here S is the order parameter, E_γ is the activation energy equal 0.27 eV (see Fig. 5). Both E_f and E_γ describe the processes associated with rotation of long molecular axes; however, E_f and E_γ are different, most probably because E_f describes flip-overs of a single molecule while E_γ is associated with a small angle rotation of many molecules.

3. FAST MODULATION OF OPTICAL RETARDATION

The original idea [5] of this work was to employ the DFN in a geometry in which the electric field yields a substantial reorienting torque in both the
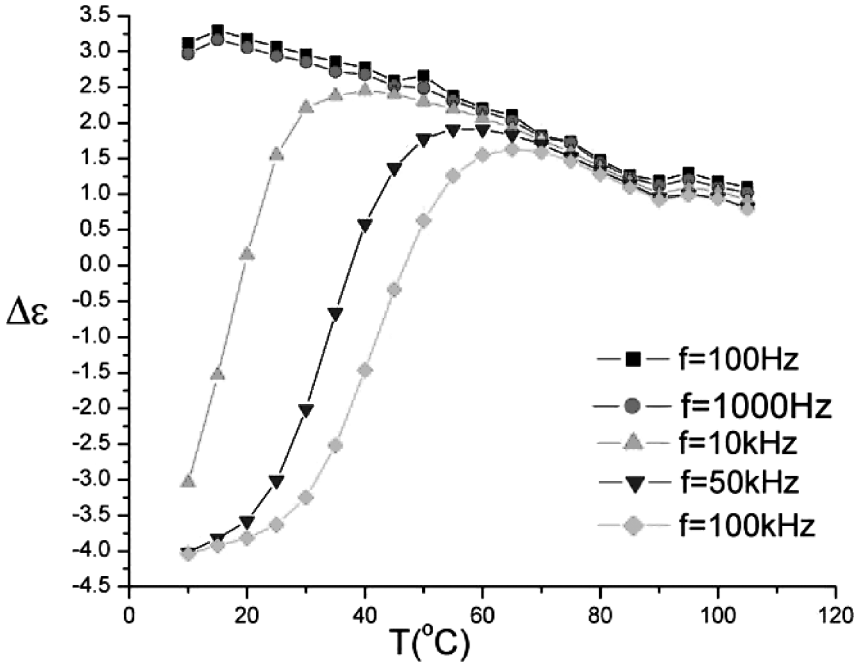
FIGURE 3 Dielectric anisotropy Δε as a function of the cell temperature T.

processes of director reorientation toward the planar state and the homeotropic state. A suitable geometry would be the one with a high pre-tilt angle, say $\alpha_b = 45°$. There is no threshold of reorientation and the dielectric torque is also assisted by the surface anchoring torque when the director returns to the initial titled orientation.

We carried out the experiments at an elevated temperature $32°$C, where $f_c = 31$ kHz. This allowed us to decrease the rotational viscosity and also to use a relatively high frequency of 7 kHz to drive the cell in the "low-frequency" regime. The high-frequency driving voltage was applied at 50 kHz. The voltage dependence of phase retardation was measured in a standard fashion, with the DFN cell of thickness $d = 14.5$ μm placed between two crossed polarizers, Figure 6.

The projection of director **n** onto the cell substrates makes an angle $45°$ with the axes of polarizer and the analyzer, so the intensity of transmitted light follows the rule: $I = I_0 sin^2 \pi \Delta L / \lambda$, where I_0 is the intensity of incident light (we neglect small corrections caused by reflection at interfaces, scattering at director fluctuations, etc.) and λ is wavelength of the light [3]. Figure 6 shows I (top trace) vs. applied voltage U_{rms} at frequencies 7
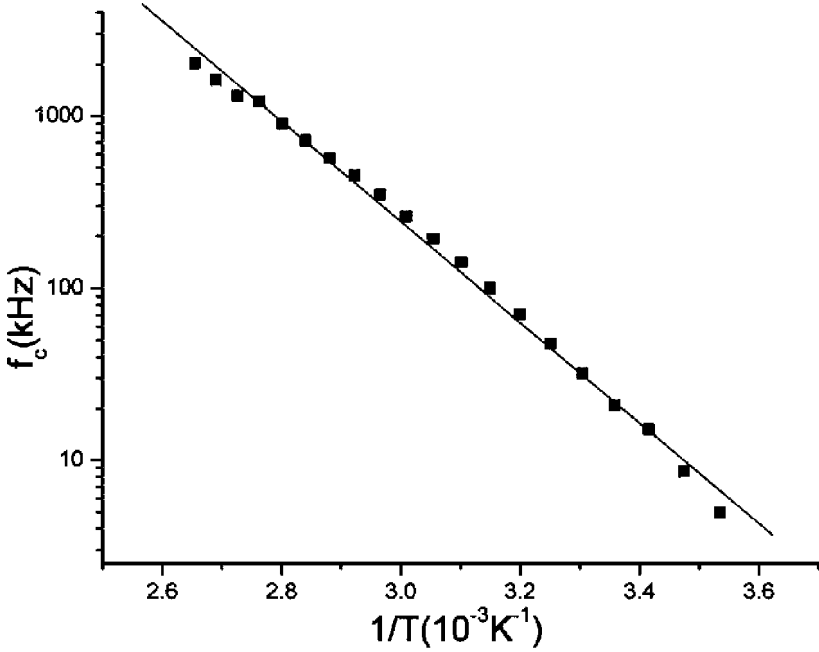
FIGURE 4 Crossover frequency f_c (logarithmic scale) vs. the inverse temperature $1/T$.

and 50 kHz (bottom trace). The variation of I between the two neighboring minima (e.g., A and B in Fig. 6) corresponds to the retardation shift $\Delta L_{AB} = 633$ nm. A larger shift $\Delta L_{CD} = 2.5\,\mu\text{m}$ is achieved between the states C and D.

As follows from the theory, see Reference [5], the switching time can be dramatically shortened by applying large-amplitude voltage signals to the cell at both frequencies, as the value of *FoM* increases at high voltages:

$$FoM \approx \frac{K(n_e - n_o)^2}{1.2\gamma_1}\left(1 + \frac{U_{rms}^2}{U_c^2}\right) \tag{7}$$

We optimized the driving scheme for DFN cell by including special short pulses (SSPs) of high-amplitude (at both driving frequencies) to initiate fast director reorientation, followed by a relatively low voltage to keep the retardation at the desired level. The oscilloscope pictures of fast switching at relatively small ($\Delta L_{OA} \approx 0.3\,\mu\text{m}$) and large ($\Delta L_{CD} = 2.5\,\mu\text{m}$) optical retardations are demonstrated in Figures 7 and 8, respectively. In Figure 7, the first SSP (duration $100\,\mu\text{s}$, $U_{rms} = 50\,\text{V}$) triggers fast
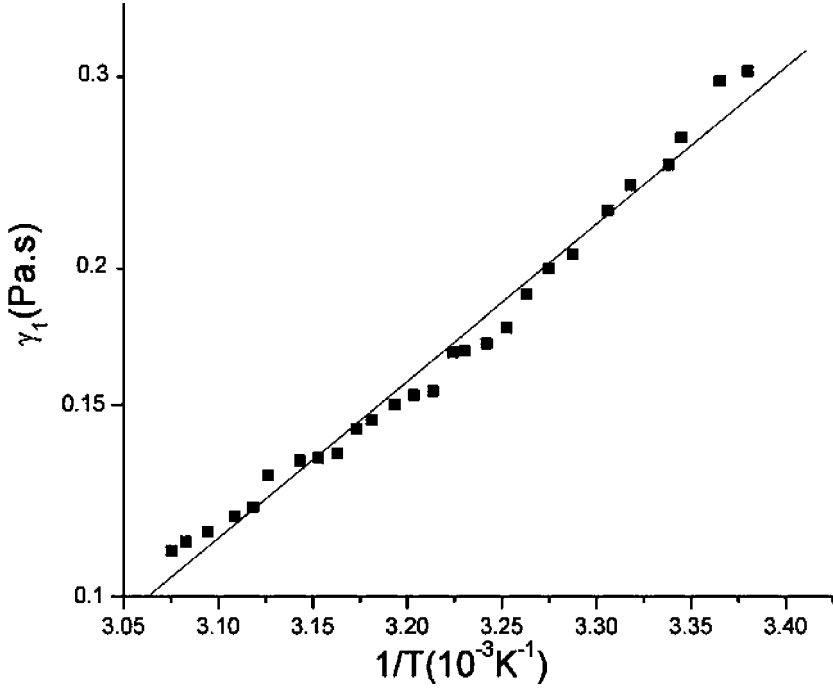
FIGURE 5 Rotational viscosity γ_1 (logarithmic scale) vs. the inverse temperature $1/T$.

reorientation towards the homeotropic state. A square-wave holding voltage $U_{rms} = 2\,\mathrm{V}$ at $7\,\mathrm{kHz}$ follows to hold the cell in the state A (the states are labeled as in Fig. 1). The A state is switched back into the initial O state by a second SSP (duration $120\,\mu\mathrm{s}$, $U_{rms} = 25\,\mathrm{V}$ at $50\,\mathrm{kHz}$); the holding voltage is zero for the state O.

Figure 8 shows $C \leftrightarrow D$ transition, switched with SSPs of $100\,\mathrm{V}$ amplitude. The switching times are $\sim 0.5\,\mathrm{ms}$. We use a short duration SSP pulse to minimize dielectric heating of the cell. Some features of fast switching are worth mentioning. First, there is a small time delay (30–$50\,\mu\mathrm{s}$) between the initial front of an SSP and the corresponding front of the photodiode signal, Figures 7, 8 [5]. Second, the transient maxima and minima seen in Figure 8 are relatively small (meaning that the modulation of light intensity is not complete). There are few possible reasons of this effect: (a) in-plane non-homogeneity of pre-tilt angle, anchoring energy, surface viscosity, etc.; (b) the structural transition can be accompanied by an in-plane flow, which in turn may cause director dynamics.
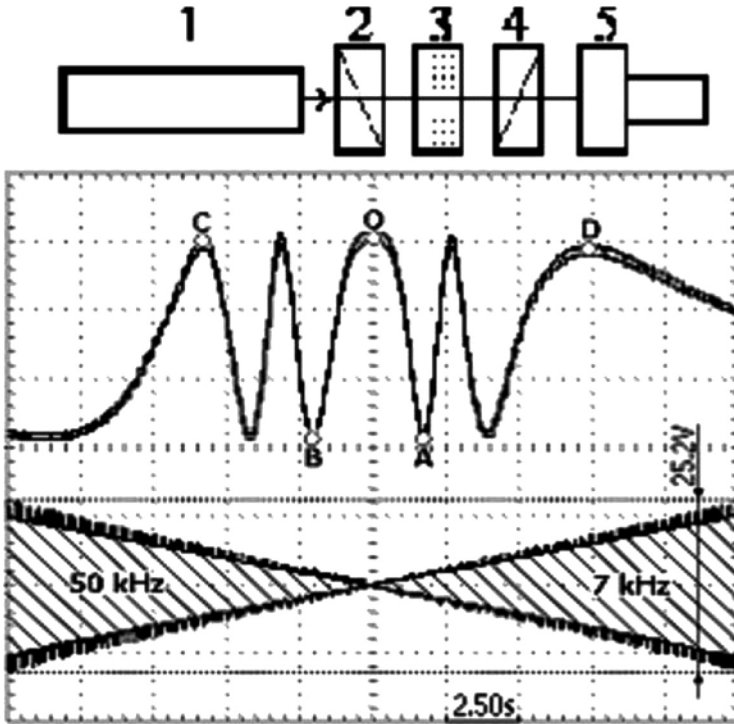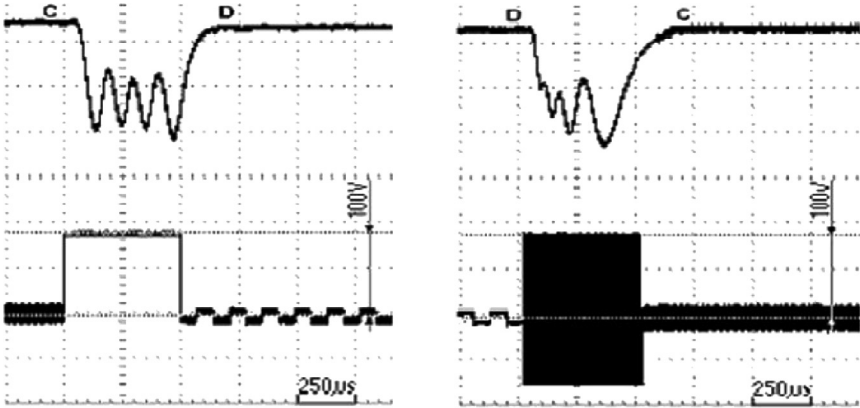
FIGURE 6 Optical setup: 1-He-Ne laser (633 nm), 2-polarizer prism, 3-DFN cell, 4-analyzer prism, 5-photodiode and the optical retardation (top) vs. applied voltage (bottom).
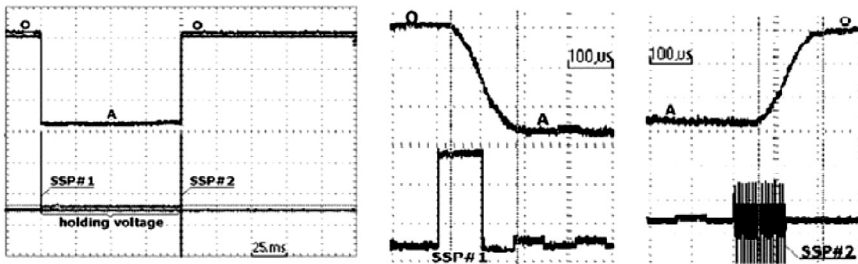
FIGURE 7 Fast phase shift by $\Delta L = 0.3\,\mu m$ driven by holding voltage $7\,kHz$ and two SSPs.

FIGURE 8 Fast switching by $\Delta L = 2.5\,\mu m$ during $\tau \approx 0.5\,ms$.

To conclude this section, we demonstrate experimentally that the chosen cell design with the high pre-tilt angle is preferable than the regular cells with either planar or homeotropic alignment. As seen from Equation (2) and (7), the response time is dependent on the elastic constant K, and one can expect that the homeotropic cell might have a faster response than a cell with either planar or high pre-tilt alignment, as the corresponding splay constant is generally smaller than that of bend. Table 1 demonstrates that the homeotropic cell is indeed capable of the fastest response, but there is a drawback as it is hard to achieve a uniform director reorientation. Even in the cells with rubbed homeotropic alignment layers, the director experiences in-plane distortions upon reorientation from the homeotropic to planar (or tilted) state. As the result, the cells with a high pre-tilt angle such as described in this work are the best overall choice.

4. DIELECTRIC HEATING

Dielectric heating is an important factor that might influence the performance of DFN cells. It affects all dielectric parameters because the Debye-type relaxation [11] is sensitive to temperature. To detect the temperature

TABLE 1 Comparison of Response Times for Different Surface Alignments

|	Planar	High Pre-tilt	Homeotropic
$\tau_{\text{off}}/d^2 (10^9\,\text{s/m}^2)$	2.48	2.43	1.42

changes in the cell, we used E-type thermocouple CHCO-0005 (Omega Inc.) with 0.05°C accuracy and head size 32 μm. We assembled 45 μm thick planar cell with etched electrodes on substrates. The head of the thermocouple was incorporated in the cell outside the electrode area, but as close as possible to it (within 1 mm).

To describe the dielectric heating effect in the nematic cell we measure the stationary temperature change ΔT with respect to the room temperature with applied voltage of various amplitudes and frequencies. Usually, ΔT reaches a stationary level within 100 s and is determined by the stationary heat flux out of the cell, as described by
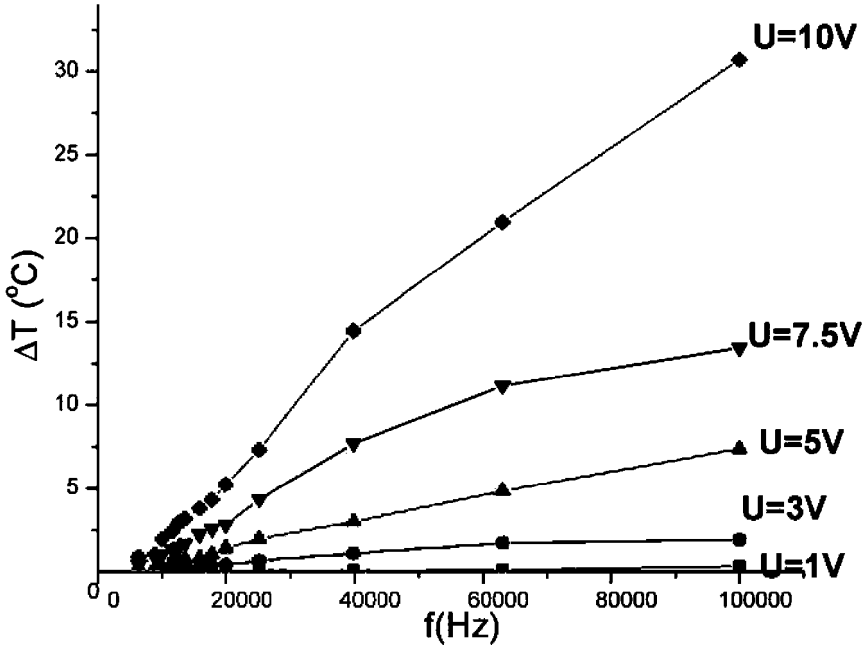
$$\Delta T = P/G. \tag{8}$$

Here G is the effective heat conductivity of the cell (including the glass substrates, the nematic layer and the possible thermal shields) and P is the power absorbed by the cell:

$$P = 2\pi A U_{rms}^2 f \varepsilon_\perp''(f)/d \tag{9}$$
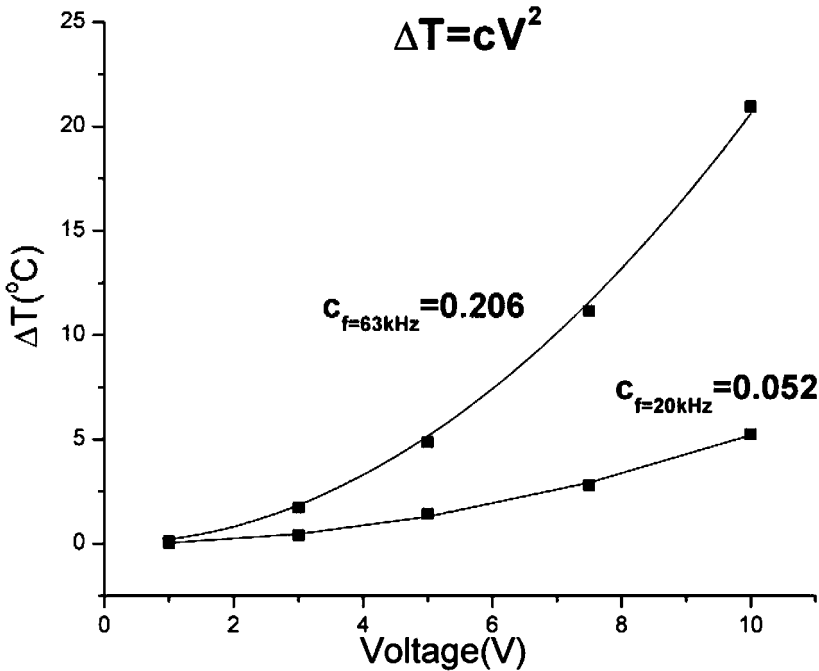
FIGURE 9 Temperature change ΔT vs. amplitude of applied voltage U$_{rms}$. Upper curve corresponds to f = 63 kHz and bottom to f = 20 kHz.

FIGURE 10 Temperature change ΔT vs. frequency of applied voltage f.

where A is the electrode area, and $\varepsilon''_\perp(f)$ is the imaginary part of the dielectric permittivity component measured perpendicularly to the director.

The experimental data in Figure 9 confirm that $\Delta T \propto U^2_{rms}$, as expected from Eqs. (8) and (9). The frequency dependence of ΔT under the condition of constant voltage amplitude is determined by $\varepsilon''_\perp(f)$: $\Delta T \propto f\varepsilon''_\perp(f)$, Figure 10. Dispersion of dielectric permittivities of LC is usually described by a Debye-type relaxation process with a relaxation time τ [12]:

$$\varepsilon''_\perp(f) = \frac{\left(\varepsilon^L_\perp - \varepsilon^H_\perp\right)f\tau}{1 + f^2\tau^2} \tag{10}$$

where $\varepsilon^H_\perp$ and $\varepsilon^L_\perp$ are the asymptotic values of $\varepsilon_\perp$ above and below the characteristic frequency $f_D = \tau^{-1}$ (Figure 1 shows that $f_D > 1$ MHz for $\varepsilon_\perp$), respectively. However, Eq. (10) provides only a qualitative description of the curves in Figure 9. Thus, either temperature dependence of τ should be taken into account in self-consistent way, or the approximation based on a single Debye-type relaxation process does not work in DFN MLC2048. Further investigations are required to clarify this issue.

We also verified that the DFN cells can be driven by high-amplitude SSPs with a high repetition rate without substantial heating-induced

changes of the switched optical retardation. For example, a DFN cell of the square aperture ($2 \times 2\,\mathrm{cm}^2$), thickness of the glass substrates 1.1 mm, and $d \approx 14.5\,\mu\mathrm{m}$, operating without any temperature-stabilizing device, was capable of switching $\Delta L \approx 1.9\,\mu\mathrm{m}$ with a repetition rate 25 Hz while driven by SSPs of amplitude $U_{rms} \approx 90\,\mathrm{V}$ and pulse duration 1 ms.

6. CONCLUSION

We demonstrated the scheme of fast optical modulator based on DFNs. We measured the temperature dependent dielectric permittivities, crossover frequency and rotational viscosity of dual frequency nematic MLC2048. We measured the response times of cells with different surface alignments and found the homeotropic cells to be the fastest; however, the optical quality of the realigned state is often poor. We analyzed the dielectric heating phenomenon, and demonstrated that this effect can be controlled to maintain the operating temperature of the cell constant.

REFERENCES

[1] McManamon, P. F., Dorschner, T. A., & Barnes, L. J. (1993). *Optical Engin.*, *32*, 2657; McManamon, P. F., Dorschner, T. A., Corkum, D. L., Friedman, L., Hobbs, D. S., Holz, M., Liberman, S., Nguyen, H. Q., Resler, D. P., Sharp, R. C., & Watson, E. A. (1996). *Proc. IEEE*, *84*, 268.

[2] Dayton, D., Browne, S., Gonglewski, J., & Restaino, S. (2001). *Appl. Opt.*, *40*, 2345.

[3] Blinov, L. M. & Chigrinov, V. G. (1994). *Electrooptic effects in liquid crystal materials*, Springer-Verlag: New York, 133–234.

[4] Wu, S. T., Neubert, M.E., Keast, S. S., Abdallah, D. G., Lee, S. N., Walsh, M. E., & Dorschner, T. A. (2000). *Appl. Phys. Lett.*, *77*, 957.

[5] Golovin, A. B., Shiyanovskii, S. V., & Lavrentovich, O. D. (2003). *SID digest*, *2*, 1472; Golovin, A. B., Shiyanovskii, S. V., & Lavrentovich, O. D. *Appl. Phys. Lett.*, to be published.

[6] Scheffer, T. J. & Nehring, J. (1977). *Appl. Phys.*, *48*, 1783.

[7] Born, M. & Wolf, E. (1999). *Principle of optics*. 7th ed. Cambridge: Cambridge, UK.

[8] Nastishin, Y. A., Polak, R. D., Shiyanovskii, S. V., Bodnar, V. H., & Lavrentovich, O. D. (1999). *J. Appl. Phys.*, *86*, 8.

[9] Chigrinov, V. G. & Grebinkin, M. F. (1975). *Krystallografiya*, *20*, 1240.

[10] de Jeu, W. H. (1980). *Physical properties of liquid crystalline materials*, Gordon and Breach: New York.

[11] Debye, P. (1929). *Polar molecules*. Dover: New York.

[12] Schadt, M. (1981). *Mol. Cryst. Liq. Cryst.*, *319*, 336.